Computational Materials Science 119 (2016) 27–32

Contents lists available at ScienceDirect

Computational Materials Science

journal homepage: www.elsevier.com/locate/commatsci

Letter

Compaction and plasticity in nanofoams induced by shock waves: A molecular dynamics study

Nina Gunkelmann [a], Yudi Rosandi [b], Carlos J. Ruestes [c], Eduardo M. Bringa [c], Herbert M. Urbassek [a,*]

[a] Physics Department and Research Center OPTIMAS, University Kaiserslautern, Erwin-Schrödinger-Straße, D-67663 Kaiserslautern, Germany
[b] Department of Physics, Universitas Padjadjaran, Jatinangor, Sumedang 45363, Indonesia
[c] CONICET and Facultad de Ciencias Exactas y Naturales, Universidad Nacional de Cuyo, Mendoza 5500, Argentina

ARTICLE INFO

Article history:
Received 13 January 2016
Received in revised form 24 March 2016
Accepted 27 March 2016

Keywords:
Shock wave
Foam
Molecular dynamics
Compaction

ABSTRACT

Shock waves are produced in Al nanofoams by a piston moving with velocity U_p. They induce plastic activity in the ligaments before eventually the foam structure is crushed and a compact material results. We demonstrate dislocation formation in the foams and correlate it with the velocity and stress profiles in the shock wave. The profiles exhibit a 3-wave structure indicating 3 wave regimes: elastic precursor, plastic activity in the ligaments, and foam crushing. The shock wave velocity V follows well macroscopic predictions, $V \propto U_p$. The length of the non-collapsed part of the foam is well described by an analytical compaction model.

1. Introduction

Metal foams receive high interest due to their light weight and high stiffness [1]. Applications range from automotive industry [2] to space science where foams may become important as radiation shields [3]. The possibility of achieving light-weight yet high-strength nanofoams make them promising candidates for their application to high-velocity impact loading conditions [4,5].

However, the mechanisms of shock response of foams – in particular nanofoams – are still not fully understood. Most experimental and simulation studies deal with macroscopic metal or plastic foams [6–8]. Finite-element models are widely used to explore stress–strain curves for metal foams [9,10]. Theoretical analysis has provided a macroscopic model of the propagation of stress waves in cellular solids [10] as well as of one-dimensional plastic shock waves [11,12]. Lopatnikov et al. investigated analytical solutions for dynamic deformation and energy absorption of foam materials under plate impact conditions under simplified materials models [13–15]. These models have been further refined in recent years to understand the dynamics of foam compaction under compression [9–17].

Molecular dynamics (MD) simulation offers a tool to investigate the atomistic response of foams to the passage of a shock wave. Zhao et al. [18] considered shock induced melting and found internal jetting producing shock front roughening [18]. Rodriguez-Nieva et al. [19] studied the plastic deformation of nanoporous fcc metals using MD and dislocation analysis and found that nanovoid surfaces act as effective sources for dislocations. Sun et al. [20] investigated the plastic response of a nanoporous Au foam to uniaxial tensile deformation on an atomistic level and Ngo et al. [21] reported on the immediate onset of plastic yielding at the smallest loads. Finally, Farkas et al. [22] used MD to study the compaction mechanisms under compression and tension. Jian et al. [23] and Zhao et al. [24] studied shocks in nanoporous Cu foams with pore size and ligament thickness of around 3.5 nm; these studies focused on the melting behavior induced by pore collapse. Also the work of Soulard et al. [25] studied shock-induced melting in Cu foams and related it to the plastic work done during pore collapse.

In the present paper we use MD simulations to study the propagation of shock waves through an Al nanofoam. We characterize the structure of the shock wave in its velocity, stress and density changes. In front of the crushing regime in which the foam material is compressed to almost bulk density, we characterize a plastic regime, in which dislocations are created in the foam ligaments. The length of the non-collapsed part of the foam as well as the shock-wave velocity can be described by simple models.

2. Simulation method

In the present paper we use MD simulations to study the propagation of shock waves through an Al nanofoam. We

* Corresponding author.
E-mail address: urbassek@rhrk.uni-kl.de (H.M. Urbassek).
URL: http://www.physik.uni-kl.de/urbassek/ (H.M. Urbassek).

http://dx.doi.org/10.1016/j.commatsci.2016.03.035
0927-0256/

construct foams with different initial filling factors varying from $\phi_0 = 0.15$ to $\phi_0 = 0.75$. The construction algorithm makes use of the non-simply connected structure of atoms of defined temperature in a liquid. In detail, we first create a template for the foam structure by starting with an fcc crystal with periodic boundary conditions. The atoms interact with a simple Lennard–Jones (LJ) potential. The target crystal is heated above the melting point for several thousand time steps to establish thermal equilibrium. Due to equilibrium fluctuations not all atoms have the same temperature. From the melt all atoms with temperature above a chosen value are removed, until the desired filling factor is met. In this stage we obtain a spongy structure, which mimics a nanofoam; however, some atoms are isolated inside voids. In order to attach them to ligaments, we relax the structure using a short-ranged LJ potential with a strongly increased binding energy. Finally, all non-connected atoms and clusters are stripped off by using a cluster detector [26] which isolates the largest interconnected structure. This structure is used as template to create the actual crystalline Al foam by using it as a spatial filter to remove all superfluous atoms from an fcc Al crystal. At two opposing surfaces we fix full-density ends of 15 nm length to the foam, which can be used as piston. We note that the use of such 'sandwiched' foam structures is widespread [27]. The average ligament size is around 2.5 nm. An example of the structures formed is given in Fig. 1(a). The foams have a rod-like shape with a long axis – denoted by z in the following – of 156 nm in total and lateral dimensions of 13 nm. The Al crystal has a $\langle 100 \rangle$ orientation with respect to the shock direction. We apply periodic boundary conditions in lateral direction and free boundaries along the shock direction. We relax the samples using high-temperature annealing at 80% of the melting temperature for 100 ps [28]. We note that for the thinnest foam ($\phi_0 = 0.15$) we had to skip this last step since it made the foam collapse. The shock wave simulations are conducted at a temperature of 10 K in order to minimize thermal noise. The open-source MD code LAMMPS [29] is used in this work to perform the simulations. For our simulations we employ the interatomic potential for Al developed by Mendelev et al. [30].

We obtained local von-Mises stresses inside the foam before and during the shock from the local atomic virials as determined within the LAMMPS software. Evidently, stresses increase during loading, but the maximum local stress was around 15 GPa; this is far above the macroscopic stresses measured as averages in the specimen in Fig. 3 below, since local stresses concentrate in the ligaments. This analysis justifies our use of the potential by Mendelev et al. [30], since the dependence of the elastic constants under pressure is realistic in this pressure regime. We note, however, that recently Al potentials have been set up that are designed to perform realistically in particular under shock conditions [31].

Shock waves are generated by the so-called piston-driven algorithm [33,34] by giving a certain particle velocity U_p in z direction to the atoms in a thin slab (thickness of one lattice constant) on one side of the sample. Note that these atoms are not subjected to the forces of the surrounding atoms. The remainder of the system volume is simulated under NVE conditions. We consider piston velocities varying from $U_p = 0.1$ to $U_p = 0.9$ km/s. The piston velocity is increased linearly from 0 to its maximum value U_p during a ramp loading time of 15 ps and then held constant. The simulation is continued up to a total time of 80 ps.

To evaluate the results we determine various material properties in dependence of the z position in the foam. These profiles are determined by dividing the sample into small slabs with a thickness of 1.215 nm along the z direction. We calculate the velocity profile in z direction, v_z, the stress in z direction, p_{zz}, the relative density, ϕ, the temperature, T, and the shear stress, p_{shear}. The latter is defined as

$$p_{\text{shear}} = \frac{1}{2}(p_{zz} - p_{\text{trans}}), \tag{1}$$

where p_{ij} denote the components of the stress tensor, and the transverse stress is defined as

$$p_{\text{trans}} = \frac{1}{2}(p_{xx} + p_{yy}). \tag{2}$$

We measure the filling factor ϕ by counting the number of atoms in each slab normalized to the bulk density in Al.

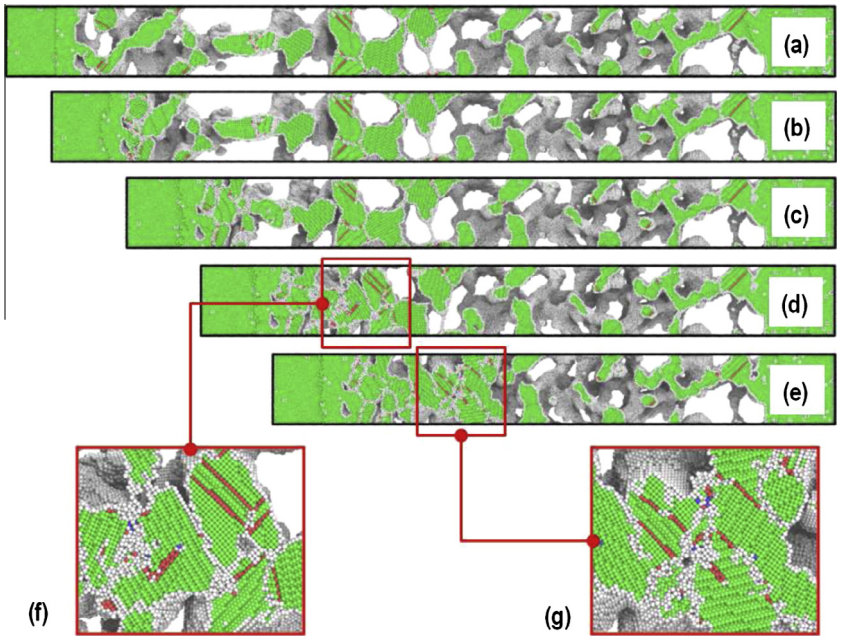

Fig. 1. Snapshots of the sample with filling factor $\phi_0 = 0.25$ at times of (a) 0 (b) 20 (c) 40 (d) 60 (e) 80 ps. (f) and (g) provide detailed views as indicated in the plot. The simulation is performed for a piston speed of $U_p = 0.7$ km/s. The shock wave runs from left to right. Local atomic structures are identified by adaptive CNA [32]. Green: fcc; red: hcp; blue bcc; gray: without defined structure. (For interpretation of the references to color in this figure legend, the reader is referred to the web version of this article.)

For visualization of the atomistic configurations we use the adaptive common-neighbor analysis together with the dislocation extraction algorithm (DXA) [35] within the free software tool OVITO [36].

3. Results

We display in Fig. 1 the shock-induced changes in our foam with initial filling factor $\phi_0 = 0.25$. In regions where the shock wave has already passed through the foam the voids collapse and the foam is compacted. Shock waves lead to defect generation, and in this case the dominant defects are stacking-fault (SF) planes in the prior fcc phase, which show as hcp atoms in the two zooms, Fig. 1(f) and (g). Large stress in the foam generates some SFs prior to shock loading, and the fraction of hcp atoms increases from 0.7% prior to loading to 1.0% at 80 ps, while the fcc fraction decreases from 80.2% prior to loading to 79.3% in the same time period.

The compacted material reaches values between 80 and almost 100% of the bulk density of Al depending on the initial density (see Fig. 3(d)).

Dislocations are formed at two stages of shock-wave response: during the plastic stage and in the crushing stage. Fig. 2 illustrates these two features. The strong plasticity set up in the crushed film is not surprising, as plasticity is required to bring about the huge shape changes needed. More interesting is the pure plastic stage, which leads to isolated dislocation formation in the ligaments in front of the crushing regime. Dislocations are mostly partials with Burgers vector $\boldsymbol{b} = \frac{1}{6}\langle 1\,1\,2\rangle$. The appearance of partials is related to the small ligament size which does not accommodate a full stacking fault ribbon.

We discuss the dynamics within the shock wave by displaying its spatially resolved characteristics for various times after launch of the shock and different initial densities ϕ_0. Fig. 3(a) shows the velocity profiles of the sample. After the ramp time, 15 ps, the piston-near part has assumed $v_z = U_p$, while at larger z the profiles show a distinct structure which is particularly well identified for lower densities, $\phi_0 = 0.25$ and $\phi_0 = 0.5$. Here we observe two changes in slope (inflection points) of the velocity profile; these have been marked exemplarily in a few cases in Fig. 3(a). We interpret this as a 3-wave structure with an elastic precursor wave, a

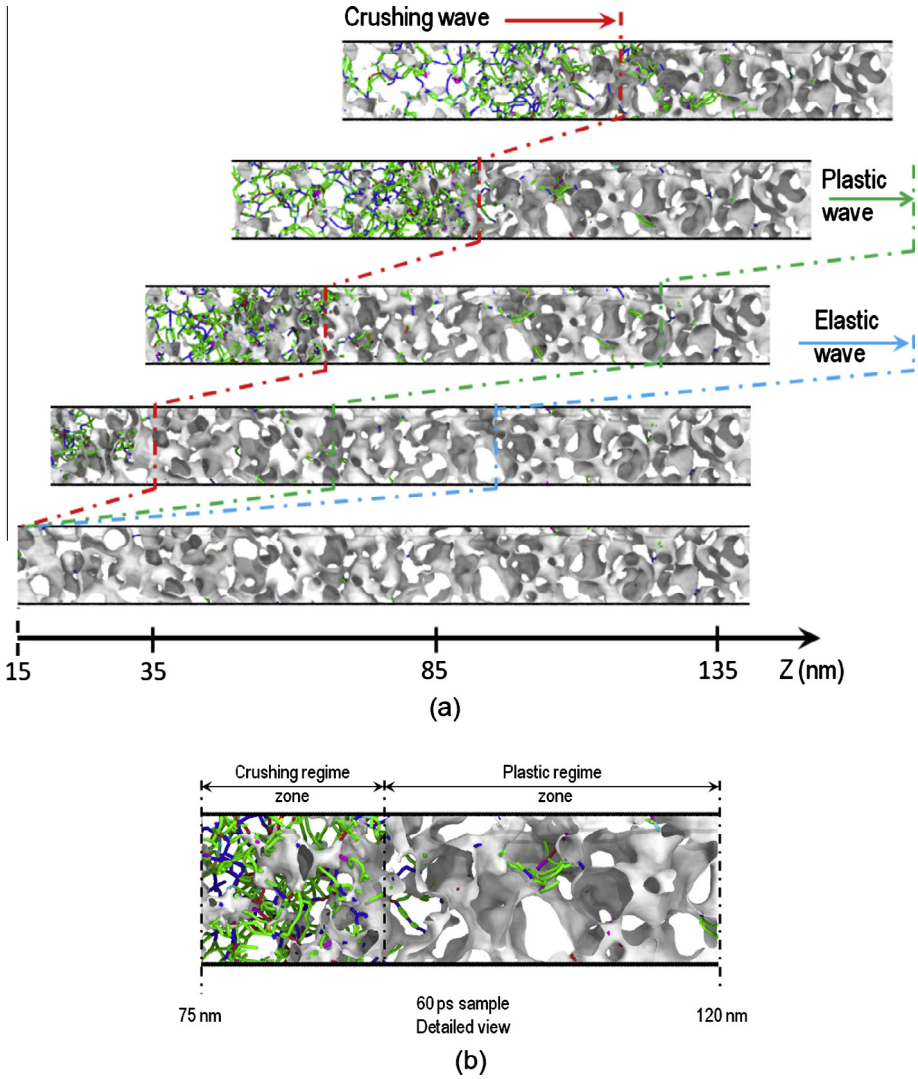

Fig. 2. (a) Dislocation pictures for $U_p = 0.7$ km/s and $\phi_0 = 0.5$ at times of 0 (bottom), 20, 40, 60 and 80 ps (top). Gray: ligament surfaces. Dislocations colored by Burgers vector: blue, perfect dislocations $\boldsymbol{b} = \frac{1}{2}\langle 1\,1\,0\rangle$; green, Shockley partials $\frac{1}{6}\langle 1\,1\,2\rangle$; magenta, stair-rod dislocations $\frac{1}{6}\langle 1\,1\,0\rangle$; yellow, Hirth partials $\frac{1}{3}\langle 1\,0\,0\rangle$; cyan, Frank partials $\frac{1}{3}\langle 1\,1\,1\rangle$; red, dislocations with unidentified Burgers vector. Picture rendered by DXA and OVITO [32]. The three-wave regime boundaries are highlighted. (b) Zoom of the 60 ps snapshot showing the emergence of dislocations in the plastic and the crushing regimes. (For interpretation of the references to color in this figure legend, the reader is referred to the web version of this article.)

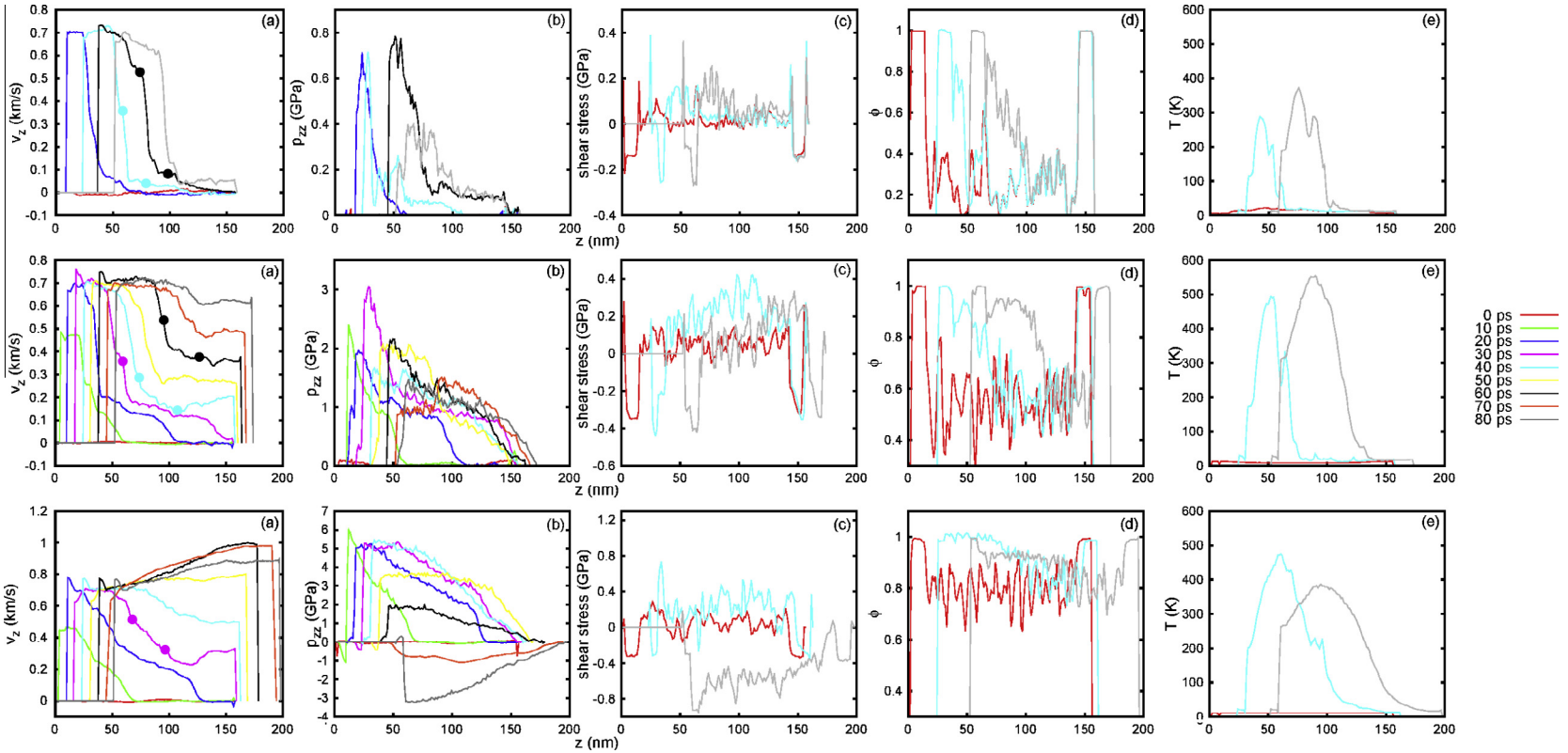

Fig. 3. Spatial profiles of the (a) atom velocity in z-direction, v_z, the (b) stress component parallel to the shock wave propagation direction, p_{zz}, (c) shear stress, Eq. (1), (d) local filling factor and (e) temperature using foams with initial filling factor $\phi_0 = 0.25$ (top), $\phi_0 = 0.5$ (middle) and $\phi_0 = 0.75$ (bottom). The simulations are performed at piston speed $U_p = 0.7$ km/s. The changes in slope in the velocity profile, v_z, (a) are exemplarily marked by dots. For clarity the profiles have not been plotted at all times.

plastic wave and a 'collapse wave'; such a structure is known for macroscopic foam compaction by shock waves [37]. In the first stage the foam is elastically deformed which is a reversible process. Then the stress is high enough for dislocation formation in the ligaments. Finally the ligaments are bent and crushed leading to the complete collapse of the foam, cf. Fig. 1. At later times the wave is reflected from the free surface at the end of the simulation slab, which is particularly well seen for the densest foam, $\phi_0 = 0.75$. After this time, the slab will end up moving as a rigid body with velocity $v_z = U_p$ (not shown).

The longitudinal stress profiles, p_{zz}, Fig. 3(b), follow the velocity profiles for small ϕ_0. For $\phi_0 = 0.25$, the stress profile at $t = 60$ ps can be compared to the snapshot of Fig. 1(d) taken at the same time; the stress maximum corresponds to the crushing region at 50–80 nm. For higher-density foams huge stresses build up reaching beyond 5 GPa; for comparison note that the ideal shear strength of Al is 2.8–3.3 GPa [38,39]. After reflection from the surface the stress maxima decrease with time; note that even sizable tensile stress builds up for $\phi_0 = 0.75$ at the latest time displayed.

Transverse (shear) stress, Fig. 3(c), is responsible for ligament bending and buckling; it is considerably smaller than the longitudinal stress. Even for the densest foam, its values reach only 0.4 GPa and are an order of magnitude smaller than p_{zz}. Its broad profile covers the entire spatial region reached by the shock wave. Also the temperature profiles, Fig. 3(e), are rather similar for the 3 densities studied here. As temperature rise is due to energy dissipation by dislocation emission and foam crushing, the temperature profiles are stretched out over the entire region covered by the shock wave. Interestingly, the maximum temperatures are similar in all 3 cases.

In Fig. 4 we show our simulation data for the shock wave velocity V as a function of the piston speed, U_p. V has been evaluated from the time dependence of the wave front in Fig. 3(a), which we define as the position where the particle velocity deviates from U_p by 10%. We note that we obtain a stationary shock velocity as long as the wave is not reflected from the far end of the simulation slab.

Fig. 4 shows that the shock velocity increases linearly with the piston velocity. This can be rationalized as follows. Let us consider mass conservation through the shock front and evaluate it in the reference frame of the shock front. Uncompacted matter (bulk filling factor ϕ_0) moves into the shock front with velocity V, while compacted matter (filling factor ϕ) is left behind with velocity $V - U_p$. Mass conservation requires $(V - U_p)\phi = V\phi_0$, and hence

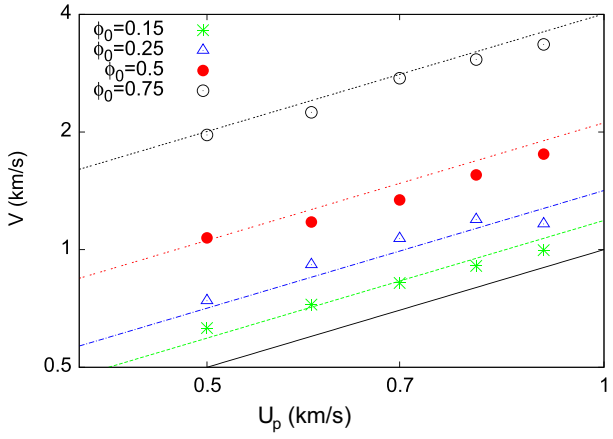

Fig. 4. Shock wave velocity V detected in the simulation (symbols) compared to the theoretical expectation, Eq. (3), as a function of the piston velocity U_p for different filling factors ϕ_0. The full line indicates the limiting behavior, $V = U_p$.

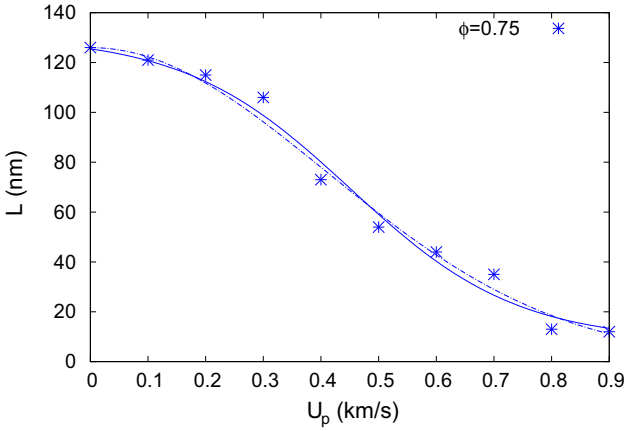

Fig. 5. Length of the non-collapsed part of the foam together with theoretical expectations of Eq. (4) (dotted) and of Eq. (5) (solid) for a foam of density $\phi_0 = 0.75$.

$$V = \frac{\phi}{\phi - \phi_0} U_p. \tag{3}$$

Strictly speaking, this relation is not linear, since ϕ itself depends on U_p. Note that a rigorous calculation of the final shock Hugoniot states is more involved, see for instance the discussion in Ref. [40]. We plot the prediction of Eq. (3) in Fig. 4 and find good agreement between theory and simulation. We note that we took $\phi = 0.85$, 0.95 and 0.99 for the thinnest ($\phi_0 = 0.25$), medium ($\phi_0 = 0.5$) and densest ($\phi_0 = 0.75$) foam; this can be read off Fig. 3(d) as the average value of the local density in the shocked region.

Total crushing of the foam is prevented by the reflection of the shock wave at the far end of the slab. We display the length of the non-collapsed part L at the end of the simulation for the densest foam, $\phi_0 = 0.75$, in Fig. 5; in this case, the shock wave passed through the entire foam even for the smallest piston velocity. L has been determined from the position in the density profile, Fig. 3(d), where the density deviates from ϕ_0 by 10%.

The data can be reasonably well fit by the model of Lopatnikov et al. [13], which has been derived for a so-called elastic-perfectly-plastic-rigid (E-P-P-R) solid:

$$L = L_0 \exp\left(-\alpha U_p^2\right). \tag{4}$$

The coefficient α depends on the density and the critical stress for collapse of the foam and $L_0 = 126$ nm is the initial length of the foam. Note that Eq. (4) has been derived from a one-dimensional model. While we apply the shock loading by means of a uniaxial strain, our foam is fully three-dimensional and so is the stress distribution, a condition that departs from the ones used to derive Eq. (4); still, we use this equation as a first-approximation representative model for analyzing our data. A fit of Eq. (4) to our data, with $\alpha = 3.00\ \mathrm{s^2\,km^{-2}}$ shows reasonable agreement. We note that the data appear to be distributed with an inverted S-shape with an inflection point at $U_p \cong 0.45$ km/s. Hence, it can be fitted by a generalized sigmoidal equation using

$$L(U_p) = a + \frac{b}{1 + \exp[(U_p - c)/d]}, \tag{5}$$

where $a = 23.13$ nm, $b = 122.54$ nm, $c = 0.45$ km/s, and $d = 0.14$ km/s.

4. Summary

Using MD simulations we studied the response of an Al nanofoam to strong shock waves. The velocity and longitudinal stress

profiles show a characteristic 3-wave structure corresponding to the 3 regimes of material response: elastic deformation, plastic response of the ligaments, and full collapse of the foam. The shock wave velocity V follows well the macroscopic prediction, $V \propto U_p$. The length of the non-collapsed part of the foam is well described by an analytical compaction model.

Future simulations might increase the system size, since the cross section and in particular the length of the present system may not be sufficiently large to reach steady-state wave propagation. Also the role of the sandwich structure used here, where the foam region is enclosed on both sides by bulk material, should be investigated, since the foam/bulk interface gives rise to wave reflection at late times.

Acknowledgments

This work has been supported by the *Deutsche Forschungsgemeinschaft* via the Sonderforschungsbereich 926. YR is grateful for funding from the Indonesian Directorate General of Higher Education (DIKTI), contract No. 393/UN6.R/PL/2015. CJR and EMB thank for support from SeCTyP-UNCuyo grant M003, and ANPCyT grant PICT-2014-0696. Simulations were performed at the High Performance Cluster Elwetritsch (RHRK, TU Kaiserslautern, Germany).

References

[1] S. Santosa, T. Wierzbicki, Comput. Struct. 68 (1998) 343.
[2] J. Banhart, Int. J. Vehicle Des. 37 (2005) 114.
[3] S.A. Thibeault, J.H. Kang, G. Sauti, C. Park, C.C. Fay, G.C. King, MRS Bull. 40 (2015) 836.
[4] G.R. Villanueva, W.J. Cantwell, Compos. Sci. Technol. 64 (2004) 35.
[5] N. Bourne, Materials in Mechanical Extremes, Cambridge Univ. Press, 2013.
[6] R.R. Boade, J. Appl. Phys. 39 (1968) 5693.
[7] P.J. Tan, J.J. Harrigan, S.R. Reid, Mater. Sci. Technol. 18 (2002) 480.
[8] R. Dezulian, F. Canova, S. Barbanotti, F. Orsenigo, R. Redaelli, T. Vinci, G. Lucchini, D. Batani, B. Rus, J. Polan, et al., Phys. Rev. E 73 (2006) 047401.
[9] Z. Zheng, C. Wang, J. Yu, S.R. Reid, J.J. Harrigan, Int. J. Impact Eng. 72 (2014) 93.
[10] D. Karagiozova, M. Alves, Int. J. Solids Struct. 71 (2015) 323.
[11] D.D. Radford, V.S. Deshpande, N.A. Fleck, Int. J. Impact Eng. 31 (2005) 1152.
[12] Z. Zheng, J. Yu, C. Wang, S. Liao, Y. Liu, Int. J. Impact Eng. 53 (2013) 29.
[13] S.L. Lopatnikov, B.A. Gama, M. Jahirul Haque, C. Krauthauser, J.W. Gillespie Jr., M. Guden, I.W. Hall, Compos. Struct. 61 (2003) 61.
[14] S.L. Lopatnikov, B.A. Gama, M. Jahirul Haque, C. Krauthauser, J.W. Gillespie Jr., Int. J. Impact Eng. 30 (2004) 421.
[15] S.L. Lopatnikov, B.A. Gama, J.W. Gillespie Jr., Int. J. Impact Eng. 34 (2007) 587.
[16] Q. Fang, J. Zhang, Y. Zhang, H. Wu, Z. Gong, Int. J. Impact Eng. 82 (2015) 103.
[17] S. Gaitanaros, S. Kyriakides, Int. J. Impact Eng. 82 (2015) 3.
[18] F.P. Zhao, Q. An, B. Li, H.A. Wu, W.A. Goddard, S.N. Luo, J. Appl. Phys. 113 (2013) 063516.
[19] J.F. Rodriguez-Nieva, C.J. Ruestes, Y. Tang, E.M. Bringa, Acta Mater. 80 (2014) 67.
[20] X.-Y. Sun, G.-K. Xu, X. Li, X.-Q. Feng, H. Gao, J. Appl. Phys. 113 (2013) 023505.
[21] B.-N.D. Ngo, A. Stukowski, N. Mameka, J. Markmann, K. Albe, J. Weissmüller, Acta Mater. 93 (2015) 144.
[22] D. Farkas, A. Caro, E. Bringa, D. Crowson, Acta Mater. 61 (2013) 3249.
[23] W.R. Jian, B. Li, L. Wang, X.H. Yao, S.N. Luo, J. Appl. Phys. 118 (2015) 165902.
[24] F.P. Zhao, B. Li, W.R. Jian, L. Wang, S.N. Luo, J. Appl. Phys. 118 (2015) 035904.
[25] L. Soulard, N. Pineau, J. Clerouin, L. Colombet, J. Appl. Phys. 117 (2015) 115901.
[26] S.D. Stoddard, J. Comput. Phys. 27 (1978) 291.
[27] J. Banhart, H.-W. Seeliger, Adv. Eng. Mater. 14 (2012) 1082.
[28] N. Gunkelmann, E.M. Bringa, K. Kang, G.J. Ackland, C.J. Ruestes, H.M. Urbassek, Phys. Rev. B 86 (2012) 144111.
[29] S. Plimpton, J. Comput. Phys. 117 (1995) 1. <http://lammps.sandia.gov/>.
[30] M.I. Mendelev, M.J. Kramer, C.A. Becker, M. Asta, Philos. Mag. 88 (2008) 1723.
[31] L. Wang, J.C. E, Y. Cai, F. Zhao, D. Fan, S.N. Luo, J. Appl. Phys. 117 (2015) 084301.
[32] A. Stukowski, Model. Simul. Mater. Sci. Eng. 20 (2012) 045021.
[33] B.L. Holian, P.S. Lomdahl, Science 280 (1998) 2085.
[34] E.M. Bringa, K. Rosolankova, R.E. Rudd, B.A. Remington, J.S. Wark, M. Duchaineau, D.H. Kalantar, J. Hawreliak, J. Belak, Nature Mater. 5 (2006) 805.
[35] A. Stukowski, K. Albe, Model. Simul. Mater. Sci. Eng. 18 (2010) 085001.
[36] A. Stukowski, Model. Simul. Mater. Sci. Eng. 18 (2010) 015012. <http://www.ovito.org/>.
[37] H. Tan, S. Qu, in: H. Altenbach, A. Öchsner (Eds.), Cellular and Porous Materials in Structures and Processes, CISM International Centre for Mechanical Sciences, vol. 521, Springer Vienna, 2010, pp. 309–334.
[38] S. Ogata, J. Li, S. Yip, Science 298 (2002) 807.
[39] D.M. Clatterbuck, C.R. Krenn, M.L. Cohen, J.J.W. Morris, Phys. Rev. Lett. 91 (2003) 135501.
[40] B. Arman, S.-N. Luo, T.C. Germann, T. Cagin, Phys. Rev. B 81 (2010) 144201.